

Journal of Climate

Non-linear radiative response to patterned global warming due to convection aggregation and non-linear tropical dynamics

--Manuscript Draft--

Manuscript Number:	
Full Title:	Non-linear radiative response to patterned global warming due to convection aggregation and non-linear tropical dynamics
Article Type:	Article
Corresponding Author:	Heng Quan Princeton University Princeton, NJ UNITED STATES
Corresponding Author's Institution:	Princeton University
First Author:	Heng Quan
Order of Authors:	Heng Quan Bosong Zhang Chenggong Wang Stephan Fueglistaler
Abstract:	Climate responses to global warming exhibit large dependence on the spatial pattern of sea surface temperature (SST) changes. A Green's function (GF) approach – predicting the global climate response to a complex SST change pattern as the linear superposition of the response to finite-area SST perturbations evaluated in isolation – has been used to systematically evaluate and understand the top of atmosphere (TOA) radiation response to patterned warming. However, the linear GF approach fails for TOA radiation reconstruction under future global warming scenario in coupled models. Here we show that the linear superposition of global mean TOA radiation responses to large SST warming perturbations at multiple patches (the GF approach prediction) overestimates the actual response to simultaneous multi-patch perturbation, because the linear superposition overestimates tropical large-scale convection aggregation strengthening upon localized heating that enhances longwave radiative cooling, which is further explained by the overestimation of circulation response and associated horizontal water vapor transport. The non-additivity of TOA radiation response is caused by the non-additivity of convection aggregation, ultimately rooted in non-linear tropical dynamics. We also demonstrate that the prediction error of the GF approach grows with decreasing patch size (equivalently, increasing patch number). We conclude that using the GF approach to predict future climate change would overestimate longwave radiative cooling and underestimate climate sensitivity. Our research also highlights that an increase in the degree of large-scale convection aggregation has a non-linear and negative feedback for mean warming.
Suggested Reviewers:	Paulo Ceppi Imperial College, London p.ceppi@imperial.ac.uk Adrian Tompkins International Centre for Theoretical Physics tompkins@ictp.it Prashant Sardeshmukh University of Colorado, Boulder Prashant.D.Sardeshmukh@noaa.gov Mark Zelinka Lawrence Livermore National Laboratory zelinka1@llnl.gov

Heng Quan
Program of Atmospheric and Oceanic Sciences,
Department of Geosciences, Princeton University
September 05, 2023

Dear *Journal of Climate* Editor:

Enclosed is a manuscript entitled "Non-linear radiative response to patterned global warming due to convection aggregation and non-linear tropical dynamics" that we respectfully submit for consideration for publication in *Journal of Climate*. The manuscript is coauthored by Heng Quan, Bosong Zhang, Chenggong Wang and Stephan Fueglisterler. Heng Quan will be the corresponding author. The work we present is original and has never been submitted for publication elsewhere. Thank you in advance for your time and consideration.

Sincerely,

Heng Quan
hengquan@princeton.edu



Click here to access/download

Cost Estimation and Agreement Worksheet
Journals Estimation Worksheet New Submission
Format.pdf

Generated using the official AMS L^AT_EX template v6.1

1 **Non-linear radiative response to patterned global warming due to convection**
2 **aggregation and non-linear tropical dynamics**

3 Heng Quan,^{a,b} Bosong Zhang,^b Chenggong Wang,^{a,b} and Stephan Fueglistaler^{a,b}

4 ^a *Department of Geosciences, Princeton University, Princeton, NJ, US*

5 ^b *Program in Atmospheric and Oceanic Sciences, Princeton University, Princeton, NJ, US*

6 *Corresponding author:* Heng Quan, hengquan@princeton.edu

7 ABSTRACT: Climate responses to global warming exhibit large dependence on the spatial pattern
8 of sea surface temperature (SST) changes. A Green's function (GF) approach - predicting the global
9 climate response to a complex SST change pattern as the linear superposition of the response to
10 finite-area SST perturbations evaluated in isolation – has been used to systematically evaluate and
11 understand the top of atmosphere (TOA) radiation response to patterned warming. However, the
12 linear GF approach fails for TOA radiation reconstruction under future global warming scenario
13 in coupled models. Here we show that the linear superposition of global mean TOA radiation
14 responses to large SST warming perturbations at multiple patches (the GF approach prediction)
15 overestimates the actual response to simultaneous multi-patch perturbation, because the linear su-
16 perposition overestimates tropical large-scale convection aggregation strengthening upon localized
17 heating that enhances longwave radiative cooling, which is further explained by the overestimation
18 of circulation response and associated horizontal water vapor transport. The non-additivity of TOA
19 radiation response is caused by the non-additivity of convection aggregation, ultimately rooted in
20 non-linear tropical dynamics. We also demonstrate that the prediction error of the GF approach
21 grows with decreasing patch size (equivalently, increasing patch number). We conclude that using
22 the GF approach to predict future climate change would overestimate longwave radiative cooling
23 and underestimate climate sensitivity. Our research also highlights that an increase in the degree
24 of large-scale convection aggregation has a non-linear and negative feedback for mean warming.

25 **1. Introduction**

26 In marked contrast to climate simulations with coupled atmosphere-ocean general circulation
27 models (GCMs), atmospheric general circulation model (AGCM) simulations with prescribed
28 observed sea surface temperatures (SSTs) over the historical period (late 1800s to present) show
29 large, multi-decadal variations of apparent climate sensitivity (global average surface temperature
30 change due to a radiative forcing equivalent to that from doubling atmospheric CO₂) (Andrews
31 et al. 2018, 2022). The very different behavior can be attributed to the geographical structure -
32 or "pattern" - of changes of SST over the historical record. The far-reaching consequences of this
33 disagreement between observational record and coupled GCMs demand rigorous analysis of this
34 "pattern effect" (Stevens et al. 2016). Given the potentially infinite number of possible patterns, a
35 Green's Function (GF) approach promises a computationally feasible method to better understand
36 the effect of any geographic structure of SST changes to radiative feedbacks and climate sensitivity
37 (Zhou et al. 2017; Dong et al. 2019; Lewis and Mauritsen 2021; Zhang et al. 2023; Bloch-Johnson
38 et al. 2023).

39 The premise of the GF approach is that one can predict the climate state vector Ω (with components
40 temperature, humidity, clouds, winds, etc.) change at all locations (and hence also the global
41 average) in response to an arbitrarily structured perturbation of SST as the linear superposition of
42 the linearized response to SST perturbations in small domains. In discrete form for a finite-sized
43 patch at position x_0 , the total change in the state vector $\Delta\Omega(x_0)$ is the sum of the single-patch
44 responses at each position x times the SST change at this position ($\Delta\text{SST}(x)$):

$$\Delta\Omega(x_0) = \sum_x \frac{\partial\Omega(x_0)}{\partial\text{SST}(x)} \cdot \Delta\text{SST}(x), \quad (1)$$

45 where $\Delta\text{SST}(x)$ represents the change of SST at grid box x and the partial derivatives $\frac{\partial\Omega(x_0)}{\partial\text{SST}(x)}$ are
46 calculated by localized SST warming experiments in an atmosphere model with fixed SST (Barsugli
47 and Sardeshmukh 2002; Barsugli et al. 2006). Equation 1 requires (i) that the atmosphere responds
48 to a perturbation of SST at one location linearly (the *linearity* condition), and (ii) that the responses
49 to local perturbations are linearly additive (the *additivity* condition).

50 Empirically, it has been found that the GF approach works well for the reconstruction of the
51 top of atmosphere (TOA) radiative fluxes over the historical period (Zhou et al. 2017; Dong et al.

52 2019; Lewis and Mauritsen 2021; Zhang et al. 2023), but fails for the reconstruction of the TOA
53 radiative fluxes in coupled model simulations of future global warming (e.g. $4 \times \text{CO}_2$ forcing)
54 (Zhang et al. 2023). Here, we provide a theoretical framework to explain why the GF approach
55 works in some situations but fails in others. The *linearity* assumption was examined in Williams
56 et al. (2023), and we focus on the validity of the *additivity* assumption. Much of the "pattern effect"
57 over the historical period can be traced back to the SST patterns in the tropical Pacific (Gregory
58 and Andrews 2016; Zhou et al. 2017; Dong et al. 2019; Fueglistaler 2019; Fueglistaler and Silvers
59 2021; Ceppi and Fueglistaler 2021), and correspondingly we focus on SST perturbations in the
60 tropical Pacific (from 125.5°E to 74.5°W , 22.5°N to 22.5°S). Our analysis shows that it is the
61 non-additivity of tropical large-scale convection aggregation to large SST warming perturbations
62 that breaks the additivity assumption in the GF approach. Thus, convective aggregation is not only
63 responsible for the significance of the "pattern effect", but also responsible for the failure of the
64 GF approach.

65 The paper is organized as follows. Section 2 introduces the experimental design and a metric for
66 measuring large-scale convection aggregation. Section 3 shows our main results: We first indicate
67 that TOA radiation responses to large SST warming perturbations in two adjacent tropical Pacific
68 patches are non-additive, and attribute this to the non-additivity of tropical large-scale convection
69 aggregation responses, which is further explained by the non-additivity of tropical circulation
70 responses to localized heating. Then we generalize two-patch non-additivity to multi-patch non-
71 additivity and discuss the failure of the GF approach in future global warming scenario. Finally,
72 Section 4 summarizes the main results and conclusions, and discusses the implications for efforts
73 to improve our understanding of the pattern effect and climate sensitivity.

74 2. Methods

75 a. Numerical Experiments

76 We use the Geophysical Fluid Dynamics Laboratory (GFDL) atmospheric general circulation
77 model AM4 (Zhao et al. 2018a,b) to conduct perturbation experiments forced by patch-wise SST
78 changes in the tropical Pacific, similar to the experiments of Zhang et al. (2023). AM4 uses a
79 horizontal grid spacing of approximately 100 km and outputs data with 180 grid points in the
80 meridional direction and 288 in the zonal direction (i.e. $1.0^\circ \times 1.25^\circ$ for the horizontal resolution).

81 The SST perturbations are applied to a control simulation forced by the observed climatological
82 (1982-2001) monthly means of SSTs and sea ice concentrations from the HADISST1 dataset
83 (Rayner et al. 2003). The greenhouse gas concentrations and aerosol emissions correspond to the
84 conditions of the year 2000 and are not modified in the perturbation experiments. Following Dong
85 et al. (2019), we integrate the control simulation for 45 years with the last 40-year output used
86 to compute the model's mean state. The perturbation experiments are run for 45 years, branched
87 from the fourth year of the control run (i.e. all perturbation experiments have the same initial
88 conditions). As for the control run, the first five years of the integration are discarded to allow
89 atmospheric equilibration to the perturbation, and the climatological average of the perturbation
90 simulations is calculated from the remaining 40 years.

91 Figure 1(a) shows the climatological mean SSTs and the 24 patches ($15^\circ \times 20^\circ$ each) used
92 for the SST perturbations. The patch positions are deliberately not aligned with the underlying
93 SST pattern: if the atmosphere satisfies the conditions for a GF approach, the sizes, shapes and
94 locations of the patches are not relevant other than that they constrain the set of patterns that can be
95 represented. The SST perturbations are a uniform (within a patch) +4 K or +1 K increase of SST.

96 In addition to the perturbation experiments with perpetual year 2000 conditions, we also analyse
97 an AM4 simulation with time-varying SSTs as lower boundary conditions obtained from a coupled
98 atmosphere-ocean general circulation model simulation of an abrupt quadrupling of atmospheric
99 CO₂ (labeled 4×CO₂ experiment) using the GFDL CM4 model integrated for 150 years (Zhang et al.
100 2023). The last 30 years of this experiment (when the top-of-atmosphere radiative forcing from the
101 CO₂ quadrupling has become small) are used to calculate the model's longwave radiative feedback
102 $\lambda_{\text{ref}} \approx -1.6 \text{Wm}^{-2}\text{K}^{-1}$ (clear-sky feedback $-1.85 \text{Wm}^{-2}\text{K}^{-1}$ plus cloud feedback $0.25 \text{Wm}^{-2}\text{K}^{-1}$).
103 Moreover, this simulation is used to quantify the GF approach errors for the global warming
104 following a quadrupling of CO₂.

105 b. The Gini index: a metric for large-scale convection aggregation

106 Following Zhang and Fueglistaler (2019), we use the Gini index, an economic index for inequality
107 of income, of tropical precipitation as a single-value measurement for the spatial unevenness
108 of tropical deep convection aggregation (more clustered precipitation means more aggregated
109 convection) (Pendergrass and Knutti 2018). The Gini index has been used to study the temporal

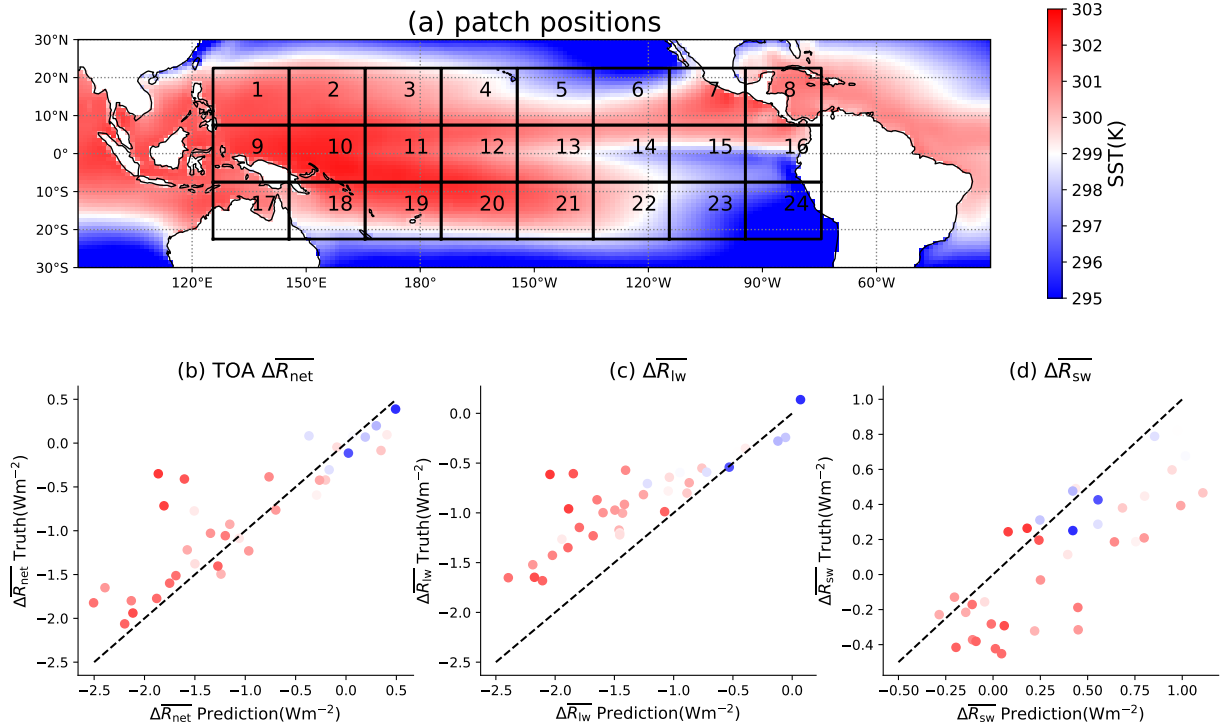
¹¹⁰ distribution of precipitation (Rajah et al. 2014). Precipitation between 30°S and 30°N are sorted in
¹¹¹ ascending order and accumulated against cumulative area. As illustrated in Fig.2(a), the Gini index
¹¹² is proportional to the shading area between the $y = x$ line and the cumulative precipitation fraction
¹¹³ as a function of cumulative area fraction. The Gini index ranges from 0 (completely uniform deep
¹¹⁴ convection) to 100 (all deep convection is located in one model grid cell). Thus, an increase in the
¹¹⁵ Gini index in a perturbation experiment indicates an increase in the aggregation of deep convection,
¹¹⁶ and *vice versa* for a decrease in the Gini index.

¹¹⁷ 3. Results

¹¹⁸ To test the validity of the *additivity* assumption in the GF approach, we calculate (i) a control run
¹¹⁹ climate state based on the climatological mean annual cycle of SST, (ii) the climate states following
¹²⁰ perturbations of SST in each patch individually by uniform +4 K and +1 K, and (iii) the climate
¹²¹ states following the perturbations of SST for a selected set of multiple patches. As expected, the
¹²² model simulations show that for very small perturbations the responses are approximately additive,
¹²³ while for perturbations of similar order as the range of tropical SST in each month (order several
¹²⁴ Kelvin), the additivity assumption of the GF approach fails. For clarity regarding the process
¹²⁵ leading to the failure of the GF approach, we show the results of +4 K experiments (non-additive)
¹²⁶ in the main text and discuss the +1 K results (approximately additive) in the supporting information.

¹²⁷ a. Non-additivity of the TOA radiative flux responses to localized SST perturbations

¹²⁸ We start from the simplest case, i.e. testing the additivity of TOA radiation responses to
¹²⁹ localized warming perturbations in two adjacent tropical Pacific patches among the 24 patches in
¹³⁰ Fig.1(a). Figure 1(b) shows the actual global mean TOA net radiative flux response $\Delta\overline{R_{\text{net}}}$ (with
¹³¹ Δ referring to perturbed minus base simulation) to simultaneous two-patch perturbation (labelled
¹³² "truth"), against the predicted change based on the linear superposition of two individual responses
¹³³ (labelled "prediction"), for 37 pairs of adjacent patches. Generally, and consistent with theoretical
¹³⁴ intuition based on the correlation between warm SST and deep convection (Zhang 1993; Sobel et al.
¹³⁵ 2002; Fueglisterler 2019), the magnitude of the response is larger for perturbations in patches with
¹³⁶ higher SST. Furthermore, Figure 1(b) shows that in most cases the GF predictions overestimate the



139 FIG. 1. (a) Climatological annual mean SST (colored contours) of the control simulation, and the patches used
 140 for the +4 K experiments. (b) Change in global mean TOA net radiation ($\Delta\bar{R}_{\text{net}}$, sign convention is incoming
 141 minus outgoing radiation) following the SST perturbation in two adjacent patches ("truth", y-axis), and the
 142 prediction based on the linear superposition of the responses to the perturbations in two patches individually
 143 ("prediction", x-axis). (c) As panel (b), but for the change in TOA longwave radiation $\Delta\bar{R}_{\text{lw}}$. (d) As panel (b),
 144 but for the change in TOA shortwave radiation $\Delta\bar{R}_{\text{sw}}$. Colors in panels (b-d) indicate the average SST of two
 145 perturbed patches, colors correspond to the color bar in panel (a).

137 true responses to the two-patch SST perturbations, especially for two adjacent warm and convective
 138 patches.

146 Figures 1(c) and (d) decompose the global mean TOA net radiative flux $\Delta\bar{R}_{\text{net}}$ into the longwave
 147 flux ($\Delta\bar{R}_{\text{lw}}$, the negative of outgoing longwave radiation, OLR) and the shortwave flux ($\Delta\bar{R}_{\text{sw}}$,
 148 incoming minus outgoing)

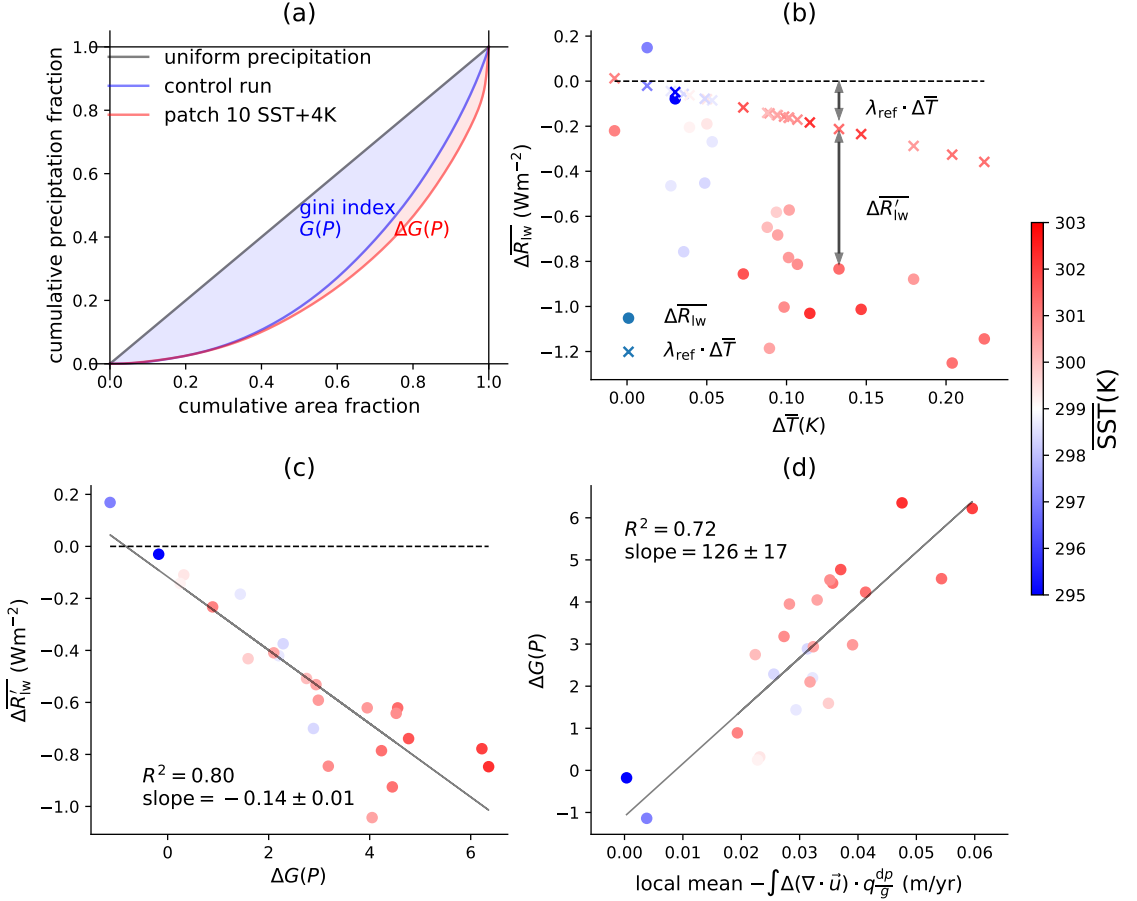
$$\Delta\bar{R}_{\text{net}} = \Delta\bar{R}_{\text{lw}} + \Delta\bar{R}_{\text{sw}} \quad (2)$$

149 Comparison of the two components shows that there is substantial, fortuitous cancellation of
150 errors in the prediction for $\Delta\overline{R}_{\text{net}}$. The errors in $\Delta\overline{R}_{\text{lw}}$ and $\Delta\overline{R}_{\text{sw}}$ are much larger than in their sum
151 $\Delta\overline{R}_{\text{net}}$, and in almost all cases the prediction substantially overestimates the true response. While
152 previously it was shown that TOA radiation responses to heating in two distant patches (one in the
153 western Pacific, the other in the eastern Pacific) are additive (Dong et al. 2019), these results show
154 that perturbations in *adjacent* patches are not additive. Also, the errors are much smaller for small
155 SST perturbations (Figure S1), further discussed in Section c. The following research will focus
156 on the non-additivity of longwave radiation response $\Delta\overline{R}_{\text{lw}}$, while shortwave $\Delta\overline{R}_{\text{sw}}$ will be briefly
157 discussed.

158 *b. The role of large-scale convection aggregation*

159 The failure of the GF approach to predict the response of, for example, global mean longwave
160 radiation, to forcing from two adjacent tropical Pacific patches can be traced to the failure to predict
161 the strength of tropical large-scale convection aggregation, or equivalently, the spatial unevenness
162 of rainfall. As discussed above, we use the Gini index of precipitation to measure the strength of
163 convection aggregation in the tropics (30°N to 30°S). Fig. 2(a) shows, as an example, the Lorenz
164 curve for the +4 K experiment in patch 10, which is in the center of the Western Pacific warm
165 pool. An increase in local SST increases precipitation locally, and on average decreases remote
166 precipitation (Fig. S4). Consequently, an increase of SST at the warm end of the SST distribution
167 strengthens tropical convection aggregation (higher Gini index, as seen for patch 10), while an
168 increase of SST at the cold end of the distribution (for example patches 23 and 24) has the opposite
169 effect (Fig. S5a). Another frequently used metric of convection aggregation, the area fraction of
170 subsidence (Bony et al. 2020), yields the same results (Fig. S5b).

175 In order to compare changes in TOA radiative fluxes due to a set of different SST perturbations,
176 we must account for the fact that the experiments only control SST but not land temperatures, and
177 a unit forcing of SST (e.g. uniform +4 K over a unit area) may correspond to different changes
178 in global mean surface temperature $\Delta\overline{T}$. Focusing on the longwave radiation component $\Delta\overline{R}_{\text{lw}}$,
179 Figure 2(b) shows $\Delta\overline{R}_{\text{lw}}$ as a function of $\Delta\overline{T}$ for each single patch +4 K simulation. The longwave
180 feedback parameter $\lambda := \Delta\overline{R}_{\text{lw}}/\Delta\overline{T}$ is different for each experiment. We can express the effective
181 longwave radiation response $\Delta\overline{R}_{\text{lw}}$ as the sum of $\Delta\overline{T}$ times the *reference* feedback parameter



171 FIG. 2. (a) Schematic of tropical (30°N to 30°S) precipitation Gini index (see section 2), a measure for
 172 convection aggregation strength. Blue: Lorenz curve and Gini index (blue shaded area) of the base simulation;
 173 red: Example of the change in the Gini index following an increase in SST in a specific patch. (b) Relation
 174 between global mean surface temperature change (x-axis) and global mean TOA longwave radiation change (y-axis)
 175 between a single-patch +4 K warming experiment and the base simulation. Each filled circle corresponds to a
 176 warming of one of the patches shown in Figure 1(a). Also shown ('x'-symbols) are the corresponding predicted
 177 changes in TOA longwave radiation based on the experiment's change in mean surface temperature multiplied
 178 with the longwave feedback parameter $\lambda_{ref} \approx -1.6 \text{ W m}^{-2} \text{ K}^{-1}$ calculated from a 4×CO₂ experiment (see section
 179 2). The difference between expected change based on the reference λ_{ref} and the experiment's true change is
 180 denoted as $\Delta \bar{R}'_{lw}$, shown for one specific simulation. (c) That difference not explained by the mean surface
 181 warming, $\Delta \bar{R}'_{lw}$ (y-axis), is highly correlated with the change in rainfall Gini index (x-axis). (d) The change in the
 182 rainfall Gini index (y-axis) is highly correlated with the change in area-normalized local (i.e. perturbed patch)
 183 mean circulation induced WVP flux convergence. Colors refer to the mean SST in the perturbed patch (color bar
 184 same to Fig. 1).

¹⁹² $\lambda_{\text{ref}} \approx -1.6 \text{ W m}^{-2} \text{ K}^{-1}$, i.e. all-sky longwave radiation feedback in a AM4 $4 \times \text{CO}_2$ experiment (see
¹⁹³ section 2), and the experiment-specific departure from the canonical $4 \times \text{CO}_2$ experiment $\overline{\Delta R'_{\text{lw}}}$:

$$\overline{\Delta R'_{\text{lw}}} = \lambda_{\text{ref}} \cdot \overline{\Delta T} + \overline{\Delta R'_{\text{lw}}}. \quad (3)$$

¹⁹⁴ Figure 2(b) shows that the magnitude of the effective response $\overline{\Delta R'_{\text{lw}}}$ of the single-patch warming
¹⁹⁵ experiments (filled circles) is substantially, and systematically, larger than what one would expect
¹⁹⁶ ('x' symbol) based on the reference feedback parameter λ_{ref} . Figure 2(c) shows that the discrepancy
¹⁹⁷ between expectation and experiment, $\overline{\Delta R'_{\text{lw}}}$, can be understood from the experiment's change in the
¹⁹⁸ rainfall Gini index: The more the rainfall Gini index $G(P)$ changes in an experiment, the larger
¹⁹⁹ the discrepancy in $\overline{\Delta R'_{\text{lw}}}$.

²⁰⁰ Consistent with previous work (Bony et al. 2016, 2020; Becker and Wing 2020; Wing et al.
²⁰¹ 2020; Zhang et al. 2021), our results show that tropical convection aggregation strengthening
²⁰² upon localized heating is associated with global mean mid-tropospheric drying (Fig. S5(c)) and
²⁰³ global mean high cloud cover reduction (Fig. S5(d); see also Radley and Fueglistaler (2014)).
²⁰⁴ By contrast, the relatively uniform warming forced by $4 \times \text{CO}_2$ has a much weaker effect on the
²⁰⁵ tropical convection aggregation strength $G(P)$ (Zhang and Fueglistaler 2019), so mid-tropospheric
²⁰⁶ humidity and high cloud fraction remain largely unchanged in the AM4 $4 \times \text{CO}_2$ simulation (Table
²⁰⁷ 1). Mid-tropospheric drying and high cloud cover reduction both increase outgoing longwave
²⁰⁸ radiation (Tropical convection aggregation weakening in patch 23 or 24 has the opposite effects),
²⁰⁹ and it follows that the longwave radiation response to localized heating is primarily due to the
²¹⁰ change in the degree of aggregation of tropical convection (Fig. 2(c)).

²¹¹ The convection aggregation response to localized heating is caused by the redistribution of
²¹² precipitation. As shown in Appendix A, the precipitation change can be decomposed according to

$$\Delta P = \Delta E - \underbrace{\int \Delta(\nabla \cdot u) \cdot q \frac{dp}{g}}_{\text{dynamical}} - \underbrace{\int (\nabla \cdot u) \cdot \Delta q \frac{dp}{g}}_{\text{thermodynamical}} - \underbrace{\int \Delta(\nabla \cdot u) \cdot \Delta q \frac{dp}{g}}, \quad (4)$$

²¹³ where ΔE is the local evaporation change, and the last three terms represent the response of
²¹⁴ horizontal WVP (water vapor path) flux convergence decomposed into a dynamical term ($-\int \Delta(\nabla \cdot$
²¹⁵ $u) \cdot q \frac{dp}{g}$), a thermodynamical term ($-\int (\nabla \cdot u) \cdot \Delta q \frac{dp}{g}$) and a covariance term ($-\int \Delta(\nabla \cdot u) \cdot \Delta q \frac{dp}{g}$).

216 Both local (perturbed region) and remote (elsewhere) mean precipitation responses are dominated
217 by the dynamical term ($-\int \Delta(\nabla \cdot \mathbf{u}) \cdot q \frac{dp}{g}$) (Figures S6 and S7), indicating that the localized SST
218 increase affects the large-scale convection aggregation mainly through a change in the large-scale
219 circulation and its associated horizontal water vapor transport. This is verified by the linear relation
220 between the change in the dynamical term and the change in the precipitation Gini index (Fig. 2d).

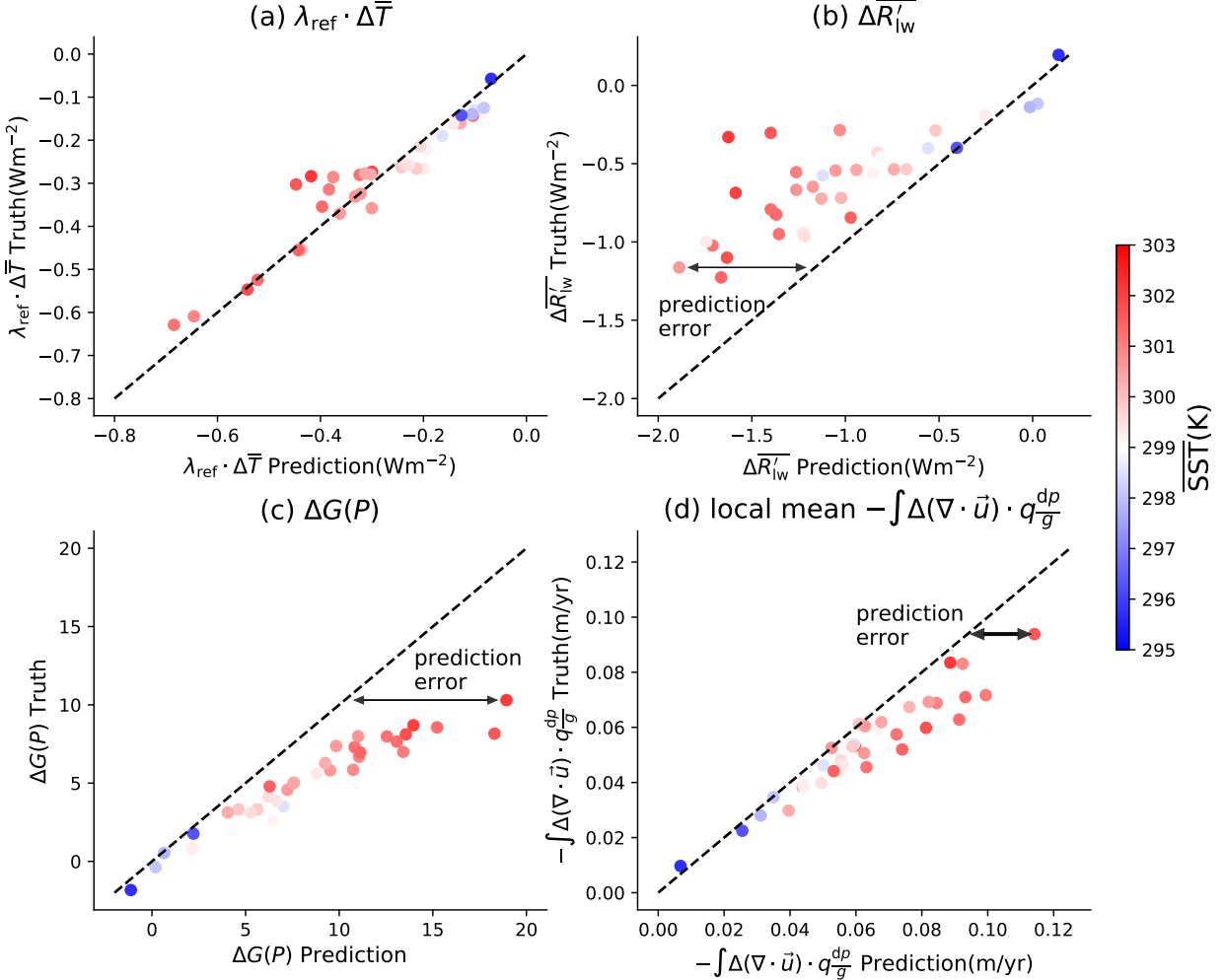
221 To summarize, the radiation response to a single-patch SST warming perturbation in the tropical
222 Pacific is mainly caused by the response of the large-scale aggregation of convection, which in turn
223 results from the change in large-scale circulation and associated water vapor transport.

224 *c. Non-additivity of convection aggregation responses to localized SST perturbations*

225 The strength of tropical convection aggregation - expressed in terms of the Gini index of tropical
226 rainfall - explains the much larger changes in $\overline{\Delta R_{lw}}$ of the single-patch experiments than expected
227 from the canonical $4 \times \text{CO}_2$ experiment. This effect is at the heart of the "pattern effect", and, as
228 we will show, also leads to the failure of the GF approach.

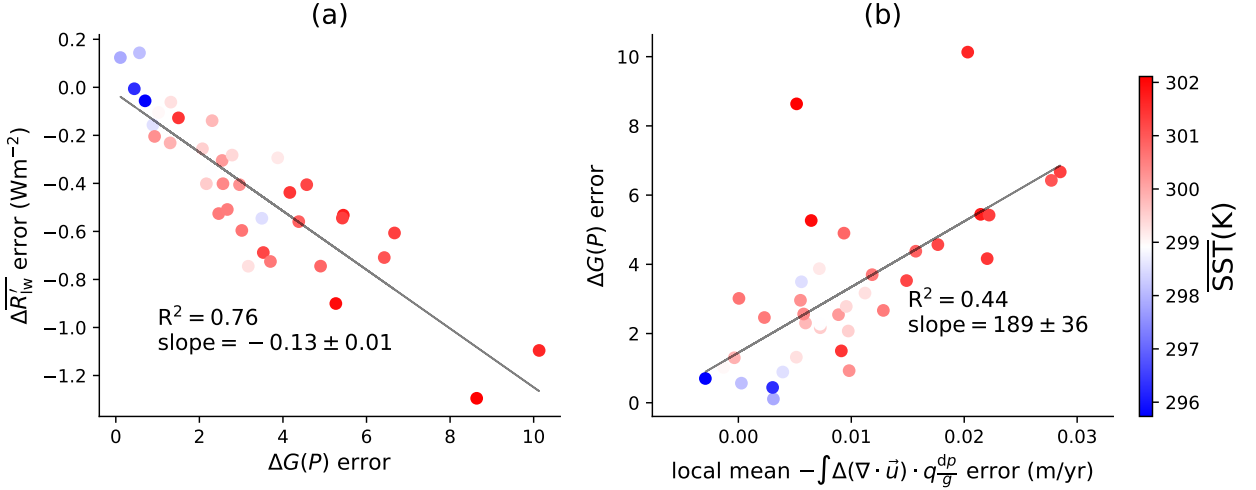
229 Figure 3 compares the results obtained from simulations with +4 K perturbations in two adjacent
230 patches ("truth") to the prediction based on the sum of the corresponding single-patch experiments
231 ("prediction"). Figure 3(a) shows that the global mean surface temperature changes $\Delta\bar{T}$ are not
232 perfectly additive, but when converted to outgoing longwave radiation by multiplication with λ_{ref} ,
233 the error in $\lambda_{ref} \cdot \Delta\bar{T}$ is small compared to the error in $\overline{\Delta R'_{lw}}$. As shown in Figure 3(b), the failure
234 in the GF reconstruction of $\overline{\Delta R_{lw}}$ is mostly due to the overestimate of $\overline{\Delta R'_{lw}}$.

241 Not surprisingly, the linear sum of the responses to individual +4 K perturbations in two adja-
242 cent patches overestimates local precipitation increase and remote precipitation decrease (Fig.S8).
243 Therefore, for most warm patches, the linear sum overestimates tropical convection aggregation
244 strengthening (Fig.3(c)), and the prediction error is larger for larger $G(P)$ change. This is in
245 turn associated with an overestimation of mid-tropospheric drying (Fig.S9a) and high cloud cover
246 reduction (Fig.S9b), ultimately resulting in the overestimation of $\overline{\Delta R'_{lw}}$. As indicated by Fig.4(a),
247 the prediction error of $\overline{\Delta R'_{lw}}$ is well explained by the prediction error of $\Delta G(P)$ (their relation is
248 almost identical to that between $\overline{\Delta R'_{lw}}$ and $\Delta G(P)$ in Fig.2(c)). Similarly, the overestimation of
249 mid-tropospheric drying (Fig.S9a) also explains the overestimation of TOA shortwave radiation
250 $\overline{\Delta R_{sw}}$ in Fig.1(d).



235 FIG. 3. Comparison of true response (y-axis) following warming ($+4\text{ K}$) in two adjacent patches to the GF
 236 approach prediction (the linear sum of responses to warming in two patches individually); of: (a) global average
 237 surface temperature, multiplied with λ_{ref} for comparison with panel (b); (b) Change in TOA longwave radiation
 238 explained by convection aggregation ($\Delta\overline{R}'_{\text{lw}}$); (c) Tropical precipitation Gini index; (d) Local (perturbed region)
 239 mean circulation induced WVP flux convergence. Colors indicate the mean SST of the two perturbed patches,
 240 color bar as in Fig.1.

257 Since the response of the degree of aggregation of deep convection to localized heating is mainly
 258 due to a circulation change and associated horizontal water vapor transport, we expect the prediction
 259 error of tropical rainfall Gini index $G(P)$ (Fig. 3c) to be explained by the error in the prediction
 260 of the WVP convergence change ($-\int \Delta(\nabla \cdot \vec{u}) \cdot q \frac{dp}{g}$) (Fig. 3d). Figure 4(b) shows that indeed the
 261 two follow closely a linear relationship (except for two outliers). While the slopes and correlations

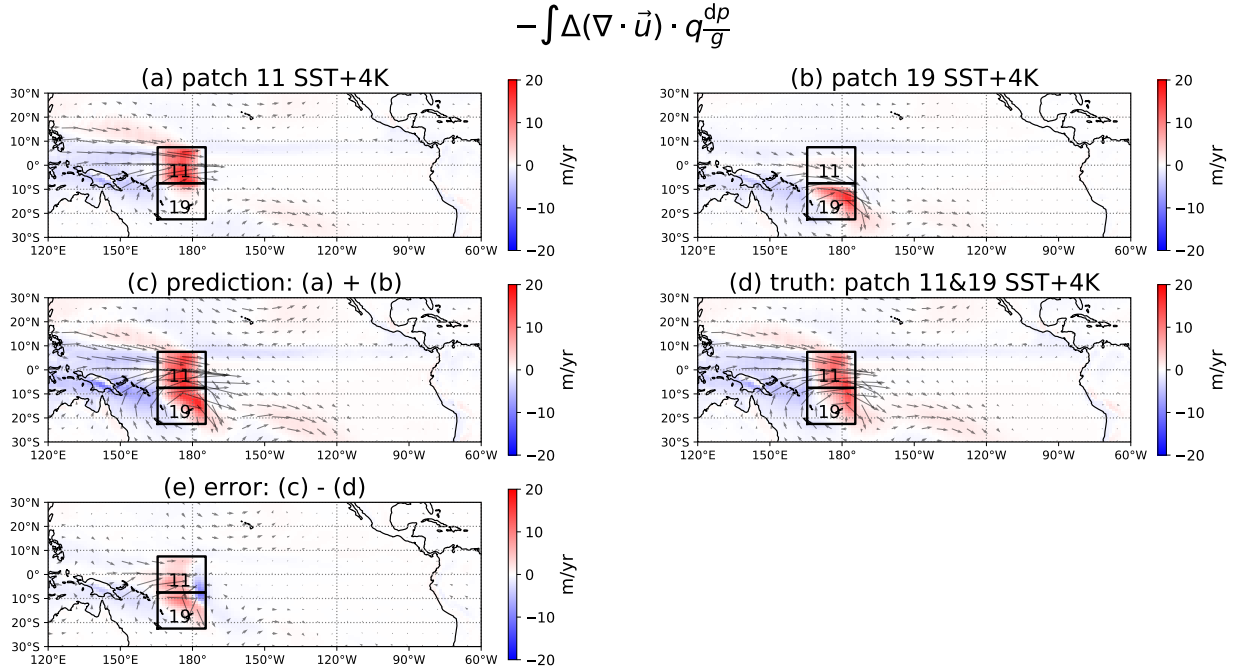


251 FIG. 4. Following Fig.3: (a) The GF approach prediction error (prediction – truth) of the change in precipitation
 252 Gini index (x-axis, as shown in Fig.3(c)) explains the prediction error of the change in TOA longwave radiation
 253 explained by convection aggregation (y-axis, $\overline{\Delta R'_{lw}}$, as shown in Fig.3(b)). (b) The GF approach prediction error
 254 of the change in local mean circulation induced WVP flux convergence (x-axis, as shown in Fig.3(d)) explains
 255 the prediction error of the change in precipitation Gini index. Colors indicate the mean SST of the two perturbed
 256 patches, color bar as in Fig.1.

262 are very similar for the relation between change in Gini index and change in $\overline{\Delta R'_{lw}}$ (Fig. 2c) and
 263 the GF prediction errors therein for the sum of two perturbed patches (Fig. 4a), the slopes and
 264 correlations differ somewhat (around one standard deviation) for the relation between Gini index
 265 and local moisture convergence (compare slopes and correlations in Fig. 2d and 4b).

266 Therefore, we conclude that the TOA radiation responses to large SST warming perturbations
 267 (+4 K) in two adjacent tropical Pacific patches are not additive because of the non-additivity of
 268 tropical large-scale convection aggregation responses (Fig.4(a)), which is further explained by
 269 the non-additivity of tropical circulation responses to localized heating (Fig.4(b)). By contrast,
 270 the radiation responses to small SST warming perturbations (+1 K) are additive (Fig.S1) because
 271 convection aggregation and circulation responses are additive (Fig. S2, the +1 K counterpart of
 272 Fig. 3).

273 The non-additivity of the radiation responses is ultimately rooted in the non-additivity of the
 274 circulation responses. In order to better understand the latter, we provide a case study using
 275 the combination of patches 11 and 19, which requires an explanation. Fig. 5 indicates that the



287 FIG. 5. Non-additivity of the circulation induced WVP flux convergence responses $-\int \Delta(\nabla \cdot \vec{u}) \cdot q \frac{dp}{g}$ (color)
288 to +4 K perturbations in patch 11 and 19. (a) patch 11 +4 K. (b) patch 19 +4 K. (c) linear sum (a) + (b). (d)
289 patch 11&19 +4 K. (e) prediction error (c) - (d). Grey arrows represent the quiver plot of $\int \Delta u \cdot q \frac{dp}{g}$. Linear
290 sum overestimates local circulation induced WVP flux convergence response, indicating tropical dynamics is
291 nonlinear upon large perturbations.

286 prediction of the circulation-induced WVP flux convergence response $-\int \Delta(\nabla \cdot \vec{u}) \cdot q \frac{dp}{g}$ based on
287 the linear sum (Fig.5(c)) of the responses to the individual perturbations shows a spatial pattern
288 similar to the actual response (Fig.5(d)), but overestimates the magnitude of the local convergence
289 (Fig. 5(e)). This result is consistent with previous results pointing out that while the tropical
290 circulation response to localized heating is linearly additive in the linearized shallow water model
291 proposed by Gill (1980), but nonlinear effects, especially nonlinear momentum transport terms,
292 are not negligible in the free troposphere (Bao et al. 2022). As shown by Lutsko (2018), the linear
293 theory by Gill (1980) works for small perturbation only while for larger perturbations the tropical
294 circulation response to localized heating is sublinear (Lutsko 2018). Correspondingly, the GF
295 approach works for the (small perturbation) +1 K perturbation (see Figure S3, the equivalent figure
296 to Fig. 5 but with +1 K perturbations).

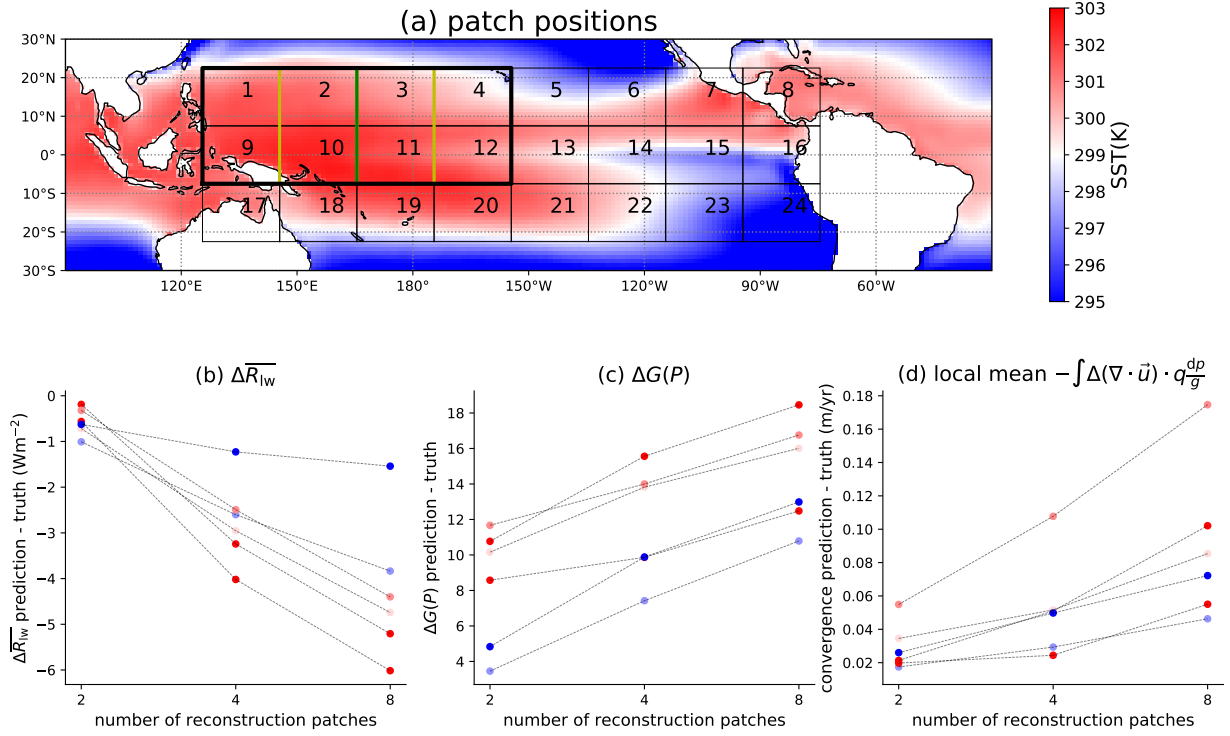
292 *d. From two-patch combination to multi-patch combination*

293 The results discussed in the previous sections suggest that - in violation of the GF conditions
294 - the size of the patch with perturbed SST matters. Forcing over a larger area leads to a weaker
295 response than expected based on the sum of the responses to smaller patch forcings, eventually
296 approaching the modest changes observed in coupled GCMs where the warming is comparatively
297 uniform (Table 1, Zhang and Fueglistaler (2019)). Consequently, we expect that the error in the
298 GF prediction is a function of the size of the perturbed patch. In order to test this hypothesis,
299 we carried out a set of simulations with SST forcing in eight neighbouring patches (patches 1-4,
300 and 9-12; see Fig. 6(a)), whereby we use the GF approach to predict the response to the forcing of
301 all eight patches based on the linear superposition of the responses to the (i) eight corresponding
302 single-patch (smallest patch size) experiments, (ii) four corresponding two-patch (intermediate
303 patch size) experiments, and (iii) two corresponding four-patch (large patch size) experiments.

311 The results shown in Figure 6(b-d) confirm the hypothesis that as a rule, the smaller the patch
312 size (equivalently, the more patches) used for the GF approach, the larger the prediction error
313 in the TOA longwave $\Delta\bar{R}_{lw}$ (panel b) radiative fluxes due to the larger error in the prediction of
314 tropical convection aggregation strength $G(P)$ (panel c), which is caused by larger error in local
315 mean circulation induced WVP flux convergence (panel d). The prediction error in $\Delta\bar{R}_{lw}$ is larger
316 than the error in shortwave radiation $\Delta\bar{R}_{sw}$ and again dominated by its $\Delta\bar{R}'_{lw}$ component (Fig. S10),
317 which also increases when we use smaller (more) patches for the reconstruction because of the
318 larger prediction error of mid-tropospheric humidity and high cloud cover (Fig. S11).

319 **4. Conclusions and outlook**

320 The GF approach promises an elegant way to analyse and understand the climate response to
321 forcing for any geographic structure of SST change, rather than the specific realization of the SST
322 field of a specific simulation or observation. The results presented in this paper show that the GF
323 approach cannot fulfill its promise: On one hand, the estimation of the local GF $\partial R / \partial SST$ with a
324 small perturbation $\Delta SST \lesssim 1 K$ satisfies the additivity condition (Figures S1), but the prediction is
325 not accurate (Williams et al. 2023) for the magnitude of SST changes ($> +1K$) of the present global
326 warming. On the other hand, an evaluation of the local GF with a perturbation of the magnitude
327 relevant for the present global warming problem ($> +1K$) gives an accurate global response to the



304 FIG. 6. Patch-number dependence (or equivalently patch-size dependence) of the GF approach prediction
 305 error. (a) As in Figure 1(a), but also showing for one eight-unit-patch area (bold black line), the split in 4
 306 two-unit-patches (yellow, green lines), and in 2 four-unit-patches (green line). GF approach prediction errors of
 307 the changes in: (b) TOA longwave, (c) precipitation Gini index and (d) local mean circulation induced WVP flux
 308 convergence as function of the number (or equivalently inverse size) of patches used to predict the response to
 309 +4 K warming over eight-unit-patches. Results shown for 6 different eight-unit-patches; symbol colors indicate
 310 the mean SST of the eight-unit-patch area, colorbar as in Fig. 3.

328 local SST change, but the responses are not linearly additive. As reported by Zhang et al. (2023),
 329 using +4 K patch warming perturbation experiments to evaluate the local GF $\partial R / \partial \text{SST}$ results in
 330 a substantial overestimation in the longwave radiation response compared to the true response of
 331 a $4 \times CO_2$ simulation. This is because the linear superposition based on equation 1 overestimates
 332 the convection aggregation strength $G(P)$, and as such overestimates mid-troposphere drying
 333 and high cloud cover reduction (Table 1) that enhance longwave cooling. Thus a GF approach
 334 is systematically biased towards overestimation of the OLR increase in response to a large SST
 335 increase, which translates to an underestimation of the climate sensitivity.

336 TABLE 1. Tropical precipitation Gini index, global mid-tropospheric relative humidity (MTH, averaged 700 hPa
 337 to 300 hPa) and high cloud amount (HCC) for a control simulation, a $4 \times \text{CO}_2$ global warming simulation, and
 338 the GF approach prediction for the $4 \times \text{CO}_2$ simulation based on the SST changes of the $4 \times \text{CO}_2$ simulation. Data
 339 from Zhang et al. (2023).

	AM4 Control	AM4 $4 \times \text{CO}_2$	GF reconstruct
tropical $G(P)$	43.9	42.0	74.3
MTH(%)	43.1	43.0	34.8
HCC(%)	37.8	37.5	30.2

340 The simulations presented here show the very strong dependency of the TOA radiative fluxes
 341 on the evenness of SSTs: the response in the TOA longwave radiation is roughly about a factor
 342 5 larger than expected from the mean surface temperature change and the reference feedback
 343 parameter λ_{ref} (Figure 2). It is for this reason that the "pattern effect" is important. Coupled
 344 General Circulation Models do not show a strong variation in the degree of aggregation, consistent
 345 with the fairly uniform changes in SSTs (Zhang et al. 2020). The results presented here show that
 346 the Green's function approach may not be used to predict the top of atmosphere radiative budget
 347 for SST perturbation of the magnitude of global warming GCM experiments. However, as also
 348 evident in the results presented in this paper, the single-patch ΔSST experiments provide highly
 349 useful information about the mechanisms of tropical convective aggregation, and how the degree
 350 of aggregation affects the TOA radiative fluxes and as such climate sensitivity.

351 *Data availability statement.* Postponed data for this research is available upon request.

APPENDIX A

Decomposition of precipitation change

354 We start from the water vapor path (WVP) budget equation

$$\frac{\partial \text{WVP}}{\partial t} = -\nabla \cdot \mathbf{Q} - P + E + r, \quad (\text{A1})$$

355 where water vapor path (WVP) is column integrated water vapor mass $\int q \frac{dp}{g}$ (q, p, g are spe-
 356 cific humidity, pressure and gravity), $\mathbf{Q} = \int \mathbf{u} \cdot q \frac{dp}{g}$ is the horizontal WVP flux with $\mathbf{u} = (u, v)$
 357 representing horizontal wind velocity. P and E means precipitation and evaporation, and r is

358 the residual term containing other processes affecting WVP. All terms in equation A1 have the
 359 dimension kgm^{-2} , and we convert it to m/yr by dividing liquid water density when presenting
 360 results below.

361 All analyses presented here are performed under steady state, i.e. $\frac{\partial \text{WVP}}{\partial t} = 0$ and equation A1
 362 reduces to

$$P = -\nabla \cdot \mathbf{Q} + E + r, \quad (\text{A2})$$

363 which states that the steady state precipitation P is the sum of horizontal WVP flux convergence
 364 $-\nabla \cdot \mathbf{Q}$, evaporation E and residual term r . Figure S12 verifies this equation in the control run. As
 365 expected, the WVP flux convergence $-\nabla \cdot \mathbf{Q}$ clearly shows the tropical rain belt and the residual
 366 term r is much smaller than the other three terms and can be neglected.

367 Our "response to localized heating" is defined as the difference between steady state control
 368 climate and steady state perturbed climate, so from equation A2 we have

$$\Delta P = \Delta(-\nabla \cdot \mathbf{Q}) + \Delta E, \quad (\text{A3})$$

369 which decomposes the precipitation response ΔP into the response of the WVP flux convergence
 370 $\Delta(-\nabla \cdot \mathbf{Q})$ and the response of the evaporation ΔE . Fig. S6 shows that the local (remote) precip-
 371 itation increase (decrease) upon localized heating is dominated by the local (remote) WVP flux
 372 convergence increase (decrease), while the response of evaporation plays a secondary role.

373 The response of the WVP flux convergence can be further decomposed

$$\Delta(-\nabla \cdot \mathbf{Q}) = \underbrace{- \int \Delta(\nabla \cdot \mathbf{u}) \cdot q \frac{dp}{g}}_{\text{dynamical}} - \underbrace{\int (\nabla \cdot \mathbf{u}) \cdot \Delta q \frac{dp}{g}}_{\text{thermodynamical}} - \underbrace{\int \Delta(\nabla \cdot \mathbf{u}) \cdot \Delta q \frac{dp}{g}}_{\text{covariance}} \quad (\text{A4})$$

374 where the three terms on the right side represent the change of WVP flux convergence due to the
 375 change of velocity/circulation (the dynamical component), specific humidity (the thermodynamical
 376 component) and their covariance. This decomposition is shown in Fig. S7, which shows that
 377 the local (remote) WVP flux convergence increase (decrease) upon a localized SST increase is
 378 dominated by $-\int \Delta(\nabla \cdot \mathbf{u}) \cdot q \frac{dp}{g}$. In other words, the response of WVP flux convergence upon a
 379 localized SST increase is dominated by the circulation change term.

380 Combining equation A3 and A4, we have

$$\Delta P = \Delta E - \underbrace{\int \Delta(\nabla \cdot \mathbf{u}) \cdot q \frac{dp}{g}}_{\text{dynamical}} - \underbrace{\int (\nabla \cdot \mathbf{u}) \cdot \Delta q \frac{dp}{g}}_{\text{thermodynamical}} - \underbrace{\int \Delta(\nabla \cdot \mathbf{u}) \cdot \Delta q \frac{dp}{g}}, \quad (A5)$$

381 where both local (perturbed region) and remote (elsewhere) mean precipitation responses are
382 dominated by $-\int \Delta(\nabla \cdot \mathbf{u}) \cdot q \frac{dp}{g}$.

383 **References**

- 384 Andrews, T., and Coauthors, 2018: Accounting for changing temperature patterns increases his-
385 torical estimates of climate sensitivity. *Geophysical Research Letters*, **45** (16), 8490–8499.
- 386 Andrews, T., and Coauthors, 2022: On the effect of historical SST patterns on radiative feedback.
387 *Journal of Geophysical Research: Atmospheres*, **127** (18), e2022JD036 675.
- 388 Bao, J., V. Dixit, and S. C. Sherwood, 2022: Zonal temperature gradients in the tropical free
389 troposphere. *Journal of Climate*, **35** (24), 4337–4348.
- 390 Barsugli, J. J., and P. D. Sardeshmukh, 2002: Global atmospheric sensitivity to tropical SST
391 anomalies throughout the Indo-Pacific basin. *Journal of Climate*, **15** (23), 3427–3442.
- 392 Barsugli, J. J., S.-I. Shin, and P. D. Sardeshmukh, 2006: Sensitivity of global warming to the
393 pattern of tropical ocean warming. *Climate Dynamics*, **27**, 483–492.
- 394 Becker, T., and A. A. Wing, 2020: Understanding the extreme spread in climate sensitivity within
395 the radiative-convective equilibrium model intercomparison project. *Journal of Advances in
396 Modeling Earth Systems*, **12** (10), e2020MS002 165.
- 397 Bloch-Johnson, J., and Coauthors, 2023: The Green's Function Model Intercomparison Project
398 (GFMIP) Protocol. *Authorea Preprints*.
- 399 Bony, S., A. Semie, R. Kramer, B. Soden, A. Tompkins, and K. Emanuel, 2020: Observed mod-
400 ulation of the tropical radiation budget by deep convective organization and lower-tropospheric
401 stability. *AGU advances*, **1** (3), e2019AV000 155.
- 402 Bony, S., B. Stevens, D. Coppin, T. Becker, K. A. Reed, A. Voigt, and B. Medeiros, 2016: Ther-
403 modynamic control of anvil cloud amount. *Proceedings of the National Academy of Sciences*,
404 **113** (32), 8927–8932.
- 405 Ceppi, P., and S. Fueglistaler, 2021: The El Niño–Southern Oscillation Pattern Effect. *Geophysical
406 Research Letters*, **48** (21), e2021GL095 261.
- 407 Dong, Y., C. Proistosescu, K. C. Armour, and D. S. Battisti, 2019: Attributing historical and future
408 evolution of radiative feedbacks to regional warming patterns using a Green's function approach:
409 The preeminence of the western Pacific. *Journal of Climate*, **32** (17), 5471–5491.

- 410 Fueglistaler, S., 2019: Observational evidence for two modes of coupling between sea surface
411 temperatures, tropospheric temperature profile, and shortwave cloud radiative effect in the
412 tropics. *Geophysical Research Letters*, **46** (16), 9890–9898.
- 413 Fueglistaler, S., and L. Silvers, 2021: The peculiar trajectory of global warming. *Journal of*
414 *Geophysical Research: Atmospheres*, **126** (4), e2020JD033629.
- 415 Gill, A. E., 1980: Some simple solutions for heat-induced tropical circulation. *Quarterly Journal*
416 *of the Royal Meteorological Society*, **106** (449), 447–462.
- 417 Gregory, J. M., and T. Andrews, 2016: Variation in climate sensitivity and feedback parameters
418 during the historical period. *Geophysical Research Letters*, **43** (8), 3911–3920.
- 419 Lewis, N., and T. Mauritsen, 2021: Negligible unforced historical pattern effect on climate feedback
420 strength found in HadISST-based AMIP simulations. *Journal of Climate*, **34** (1), 39–55.
- 421 Lutsko, N. J., 2018: The response of an idealized atmosphere to localized tropical heating:
422 Superrotation and the breakdown of linear theory. *Journal of the Atmospheric Sciences*, **75** (1),
423 3–20.
- 424 Pendergrass, A. G., and R. Knutti, 2018: The uneven nature of daily precipitation and its change.
425 *Geophysical Research Letters*, **45** (21), 11–980.
- 426 Radley, C., and S. Fueglistaler, 2014: The role of large-scale convective organization for tropical
427 high cloud amount. *Geophysical Research Letters*, **41** (14), 5259–5263.
- 428 Rajah, K., T. O’Leary, A. Turner, G. Petrakis, M. Leonard, and S. Westra, 2014: Changes to the
429 temporal distribution of daily precipitation. *Geophysical Research Letters*, **41** (24), 8887–8894.
- 430 Rayner, N., D. E. Parker, E. Horton, C. K. Folland, L. V. Alexander, D. Rowell, E. C. Kent, and
431 A. Kaplan, 2003: Global analyses of sea surface temperature, sea ice, and night marine air
432 temperature since the late nineteenth century. *Journal of Geophysical Research: Atmospheres*,
433 **108** (D14).
- 434 Sobel, A. H., I. M. Held, and C. S. Bretherton, 2002: The ENSO signal in tropical tropospheric
435 temperature. *Journal of climate*, **15** (18), 2702–2706.

- 436 Stevens, B., S. C. Sherwood, S. Bony, and M. J. Webb, 2016: Prospects for narrowing bounds on
437 Earth's equilibrium climate sensitivity. *Earth's Future*, **4** (11), 512–522.
- 438 Williams, A. I., N. Jeevanjee, and J. Bloch-Johnson, 2023: Circus Tents, Convective Thresholds,
439 and the Non-Linear Climate Response to Tropical SSTs. *Geophysical Research Letters*, **50** (6),
440 e2022GL101 499.
- 441 Wing, A. A., and Coauthors, 2020: Clouds and convective self-aggregation in a multimodel
442 ensemble of radiative-convective equilibrium simulations. *Journal of Advances in Modeling
443 Earth Systems*, **12** (9), e2020MS002 138.
- 444 Zhang, B., B. J. Soden, G. A. Vecchi, and W. Yang, 2021: Investigating the causes and impacts of
445 convective aggregation in a high resolution atmospheric GCM. *Journal of Advances in Modeling
446 Earth Systems*, **13** (11), e2021MS002 675.
- 447 Zhang, B., M. Zhao, and Z. Tan, 2023: Using a Green's function approach to diagnose the pattern
448 effect in GFDL AM4 and CM4. *Journal of Climate*, **36** (4), 1105–1124.
- 449 Zhang, C., 1993: Large-scale variability of atmospheric deep convection in relation to sea surface
450 temperature in the tropics. *Journal of Climate*, **6** (10), 1898–1913.
- 451 Zhang, Y., and S. Fueglistaler, 2019: Mechanism for increasing tropical rainfall unevenness with
452 global warming. *Geophysical Research Letters*, **46** (24), 14 836–14 843.
- 453 Zhang, Y., N. Jeevanjee, and S. Fueglistaler, 2020: Linearity of outgoing longwave radiation:
454 From an atmospheric column to global climate models. *Geophysical Research Letters*, **47** (17),
455 e2020GL089 235.
- 456 Zhao, M., and Coauthors, 2018a: The GFDL global atmosphere and land model AM4.0/LM4.0:
457 1. Simulation characteristics with prescribed SSTs. *Journal of Advances in Modeling Earth
458 Systems*, **10** (3), 691–734.
- 459 Zhao, M., and Coauthors, 2018b: The GFDL global atmosphere and land model AM4.0/LM4.0:
460 2. Model description, sensitivity studies, and tuning strategies. *Journal of Advances in Modeling
461 Earth Systems*, **10** (3), 735–769.

- ⁴⁶² Zhou, C., M. D. Zelinka, and S. A. Klein, 2017: Analyzing the dependence of global cloud
⁴⁶³ feedback on the spatial pattern of sea surface temperature change with a Green's function
⁴⁶⁴ approach. *Journal of Advances in Modeling Earth Systems*, **9** (5), 2174–2189.



Click here to access/download
Supplemental Material
Quan_JCLI_2023_SI.pdf